

Supplementary Information

Geometry structure guided photo-driven ion current through asymmetric graphene oxide membranes

Yaping Feng,^{a,b} Haoyu Dai,^{a,b} Jianjun Chen,^a Xian Kong,^{c*} Jinlei Yang,^{a,d*} and Lei Jiang^a

^a CAS Key Laboratory of Bio-inspired Materials and Interfacial Science, Technical Institute of Physics and Chemistry, Chinese Academy of Sciences, Beijing 100190, P. R. China.

^b University of Chinese Academy of Sciences, Beijing 100049, P. R. China.

^c Department of Chemical Engineering, Stanford University, Stanford, California 94305, USA

^d CAS Key Laboratory of Nanosystem and Hierarchical Fabrication, CAS Center for Excellence in Nanoscience, National Centre for Nanoscience and Technology, Beijing 100190, P. R. China.

[*] Corresponding author: Email: xiankong@stanford.edu; yjl@mail.ipc.ac.cn

Experimental Section

Synthesis of geometry-asymmetric GOMs

GO was synthesized by the modified of Hummers' method¹⁻³ through the acid oxidation of flake graphite. Then the GO dispersions ($\sim 3.5 \text{ mg ml}^{-1}$) were drop cast on a cellulose ester membrane substrate (Whatman), followed by a thermal annealing process.⁴ The asymmetric ratio is defined as the ratio of the thick side and thin side (H/h). By controlling the volume and inclination of GO solution, a series of different geometry asymmetric ratio of the resulting membranes can be obtained with the thickness of h fixed to $\sim 2 \text{ }\mu\text{m}$.

Characterization

The surface contact angle was measured using an OCA20 contact-angle system (Data Physics, Germany) at room temperature. The two ends of the geometrically asymmetric GOM were characterized by a scanning electronic microscope (SEM, Hitachi 4800). UV-vis spectrophotometer (UV-2600, SHIMADZU) was employed to measure the absorption spectrum of GO dispersion (0.33 mg ml^{-1}). X-ray diffraction tests were conducted on an X-ray diffractometer (Rigaku D/max 2500PC). XPS characterizations (TF Scientific, ESCALAB 250Xi) were used to determine the functional groups of GOMs.

Device fabrication

As schematically shown in Fig. 1e, the GO strip (L: 7 mm, W: 2 mm) was top sealed with a transparent polydimethylsiloxane (PDMS) elastomer in a two-compartment Teflon-structured electrochemical cell to avoid the solution leakage. Afterwards, the two ends of the sealed GO strip were trimmed off to connect with each solution reservoir. KCl aqueous solution was equally filled in each reservoir with concentration of $10 \text{ }\mu\text{M}$, otherwise specifically mentioned. A pair of Ag/AgCl electrodes was used to record the transmembrane ionic signals.

Electrical measurement

Light illumination was applied by a xenon lamp (Perfectlight, CHF-500W). A transparent window was placed above the GOM to select the illumination position for local irradiation. Wavelengths centered at 405-, 450-, 475-, 520-, 550-, 600-, 650- and 700-nm were obtained

by separately applying a series of optical filters in front of the light source. Photo-induced ionic current and voltage signals were recorded by a Keithley 2636B source meter (Keithley Instruments) without externally applied voltage.

Cation transference number

In the presence of transmembrane concentration difference (thick side: thin side, 10/1 μM), agar-saturated potassium chloride salt bridges were used to eliminate the imbalanced redox potential on the electrode|electrolyte interface. Ag/AgCl electrodes were used to record the current-voltage response. The diffusion potentials (E_{Diff}) were measured for a series of GOMs with geometry-asymmetric ratio from ~ 1 to ~ 4 . The value of t_+ can be calculated by⁵:

$$2t_+ - 1 = \frac{E_{Diff}}{\frac{RT}{zF} \ln\left(\frac{\gamma_{c_H} c_H}{\gamma_{c_L} c_L}\right)}$$

where R , T , z , F , γ , C_H and C_L represent the gas constant, temperature, charge valent, Faraday constant, activity coefficient of ions, high and low ion concentrations, respectively. The extremely narrow channel width coupled with negative surface charge on GO sheets render the GOM cation-selective ($t_+ > 0.93$, Fig. 1g).

S1. X-ray photoelectron spectroscopy (XPS) spectra of GOM

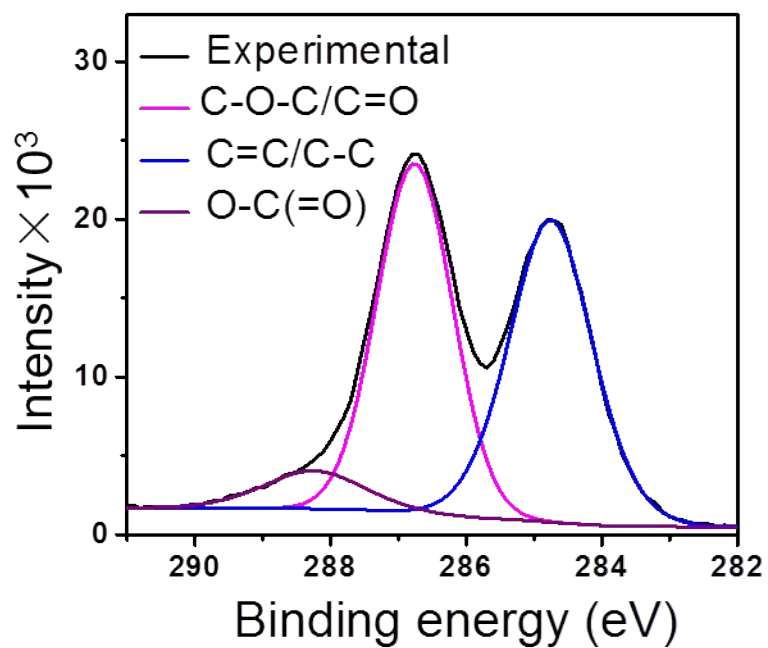


Fig. S1 XPS C-1s spectrum confirms the oxygen functional groups of GOM.

S2. The photo-responsiveness with different light intensity of a uniform GOM

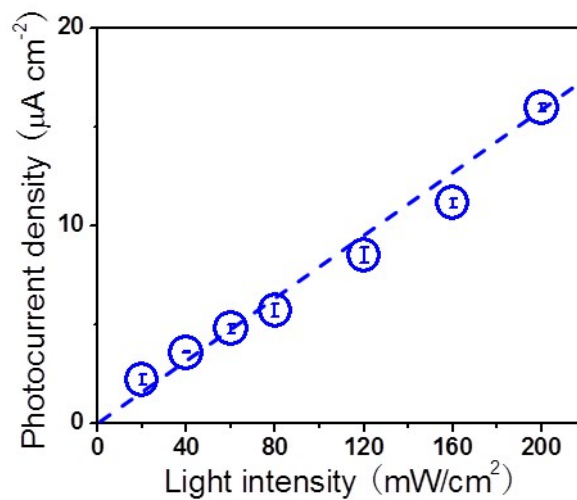


Fig. S2 The photocurrent density is enhanced with increasing the light intensity. Light illumination (100 mWcm^{-2} , 30 s duration) was applied on right $1/3$ of the thickness uniform GOM. The photocurrent density was collected in $10 \text{ }\mu\text{M}$ KCl.

S3. Photo-response in a control thickness uniform GOM sample

We also checked the photo-response of a uniform GO strip under full-area illumination as a control sample. In contrast to the geometry-asymmetric GOM, a relatively very weak photo-response was found with the control membrane sample and the photo-induced ionic current is un-controllable in the uniform GOM (Fig. S3).

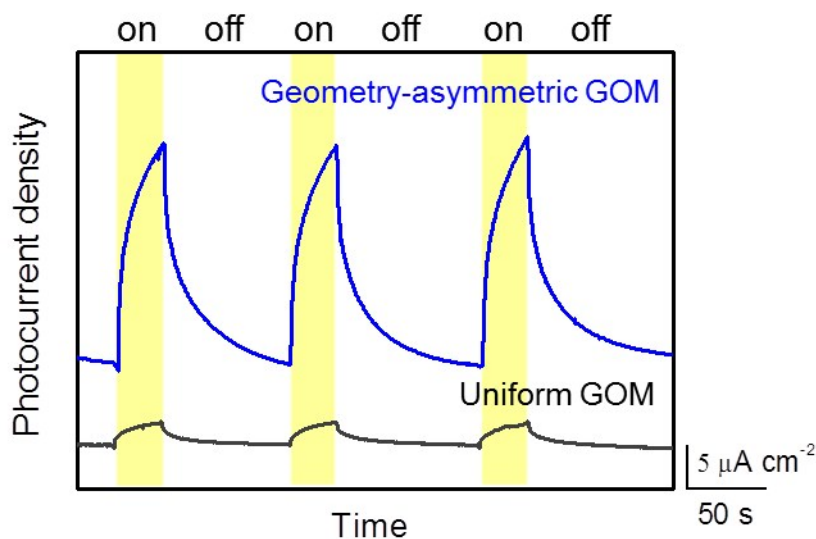


Fig. S3 Photo-response in a geometry-asymmetric GOM (asymmetric ratio: ~ 2) and a uniform control membrane sample. A very weak photo-response was found with the control sample. The photocurrent density was collected with light intensity of 100 mW cm^{-2} under full-area irradiation with illumination duration time of 30 s in $10 \mu\text{M KCl}$.

S4. The equilibrium time

Typical photocurrent density-time curves were shown in Fig. S5. We further quantify the response time of the photocurrent density trace by fitting the experimental data with an exponential function,⁶

$$J = J_0 + A \exp\left(-\frac{t}{\tau}\right)$$

where τ was the time constant, J_0 and A were fitting parameters. The time constants obtained on symmetric and asymmetric GOMs are similar. However, photocurrent density of the asymmetric GOM reaches a higher value than that of the uniform one in a fixed illumination time period, which is possibly related to more absorbed photons in the full-area irradiation.

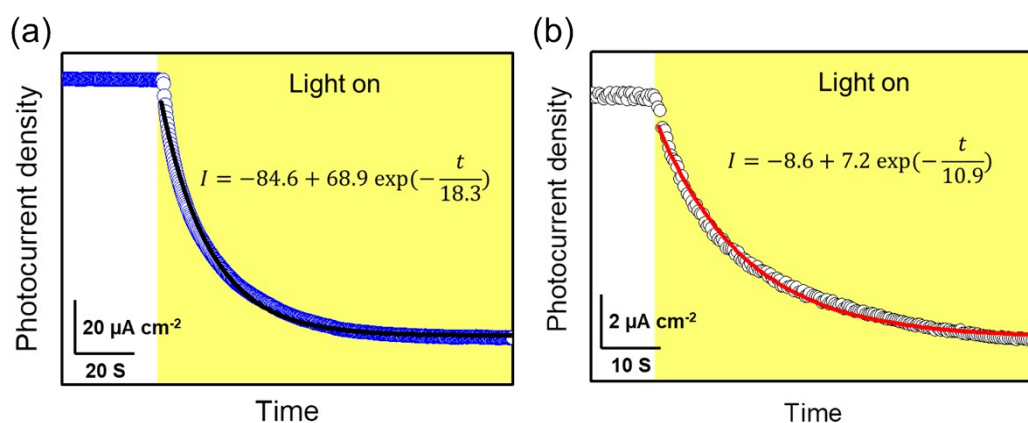


Fig. S4 (a) and (b), typical time traces of photocurrent density on symmetric and asymmetric (asymmetric ratio ~ 3.16) GOMs. The photocurrent density-time curves can be numerically fitted by an exponential function. The light intensity was 100 mW cm^{-2} . The electrolyte concentration was $10 \mu\text{M}$.

S5. Photocurrent under KCl ionic solutions with different concentrations

The value of the photocurrent density can be further enhanced by over an order of magnitude by using high-concentration electrolyte solutions.

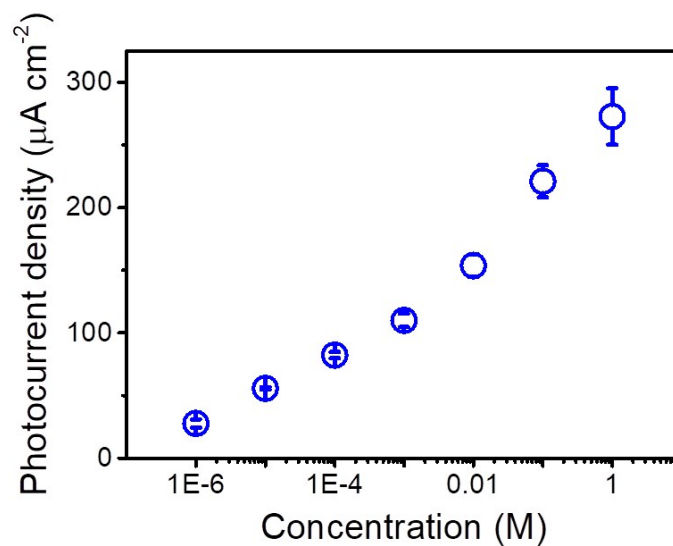


Fig. S5 Photocurrent density with respect to the electrolyte concentration. The light intensity was 100 mW cm⁻². The asymmetric ratio of the GOM was 3.16.

S6. Carrier mobility of GOM

We fabricated a GO-FET device to measure the carrier mobility (Fig. S4). The drain current increases with the gate voltage, indicating that electron-carriers are dominant in charge transport. The mobility (μ) was calculated as

$$\mu = \frac{L}{W \times (\epsilon_0 \epsilon_r / d)} \times \frac{dI_{ds}}{dV_g}$$

where L , W , ϵ_0 , ϵ_r , d , V_{ds} , I_{ds} , V_g represent the channel length, channel width, absolute dielectric constant, relative permittivity of SiO₂, thickness of SiO₂, source-drain voltage, source-drain current, gate voltage. The reported carrier mobility in GO materials varies in a wide range (10⁻⁴-10² cm² V⁻¹ s⁻¹).⁷⁻¹⁰ The estimated electron mobility $\mu_{electron}$ in our prepared GO material is $\sim 3.7 \times 10^{-4}$ cm² V⁻¹ s⁻¹ and a very small hole mobility is observed.

Einstein relation describes the transport of charge carriers in many areas including polycrystalline systems.^{11, 12} Without external voltage, the carrier diffusion coefficients (D) would dominate the carrier transport that can be correlated based on Einstein relation, $\mu = 2eD/k_B T_e$, where e and k_B are carrier charge and Boltzmann constants, T_e is carrier temperature.¹³ Therefore, there is a huge difference of diffusion rate between the holes and electrons in GOM.

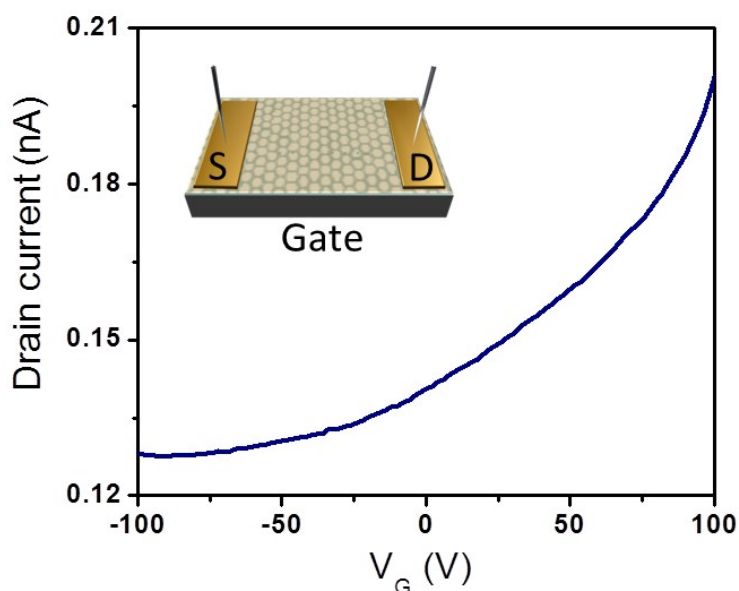


Fig. S6 Transfer characteristics ($I_{ds} - V_G$) of GO-FET device ($V_{DS} = 3$ V). L is 25 μm , W is 58 μm and d is the thickness of SiO₂ (300 nm). The diffusivity and mobility of holes are different with that of electrons for our GO samples.

S7. Anisotropic carrier transport consideration

The carrier transport in functionalized graphene-based materials occurs via variable-range hopping that involves consecutive inelastic tunneling processes between two localized states.¹⁴⁻¹⁶ At microscopic level or molecular level, charge carriers hopping between two GO plates can be categorized into three types (Fig. S7). The hopping rates of different types can be different. We also conducted several calculations with anisotropic diffusion rates in length (x) and thickness (z) direction. The degree of diffusion anisotropy is controlled by the diffusion rate in x and z directions. The results are summarized in Fig. S8, and indicate that diffusion anisotropy has minimal influence on photo-voltage generation in the macro-range.

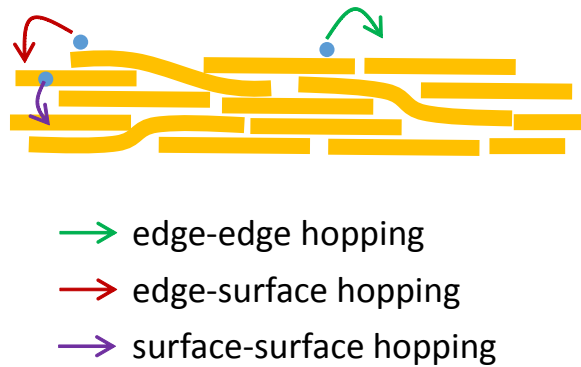


Fig. S7 Hopping pathways between two GO plates.

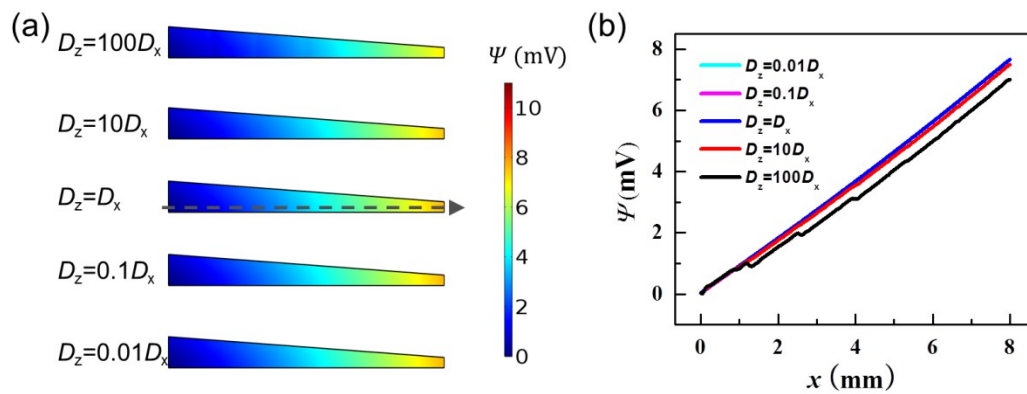


Fig. S8 Influence of anisotropic diffusion on photo-voltage. (a) Electric potential distribution for membrane with $L=8$ mm, $h=2$ μm , $H=6$ μm . The thickness and length are not to scale. (b) Electric potential along the dashed line x in panel (a). D_x is kept constant and is the same as in the main text.

S8. Potential gradient in the vertical direction

Fig. S9a replots the electric potential in $H/h=1$ membrane in a different color scale (0~50 μV) instead of the one in main text Fig. 4b. To better illustrate this, Fig. S9b and S9c plot the electric potential along the dashed line in Fig. S9a in x and z direction, respectively. In this membrane with uniform thickness, there is no electric potential change in the horizontal direction (x direction) except some negligible variations near boundaries. On the other hand, the potential change is about 50 μV in the vertical direction (z direction).

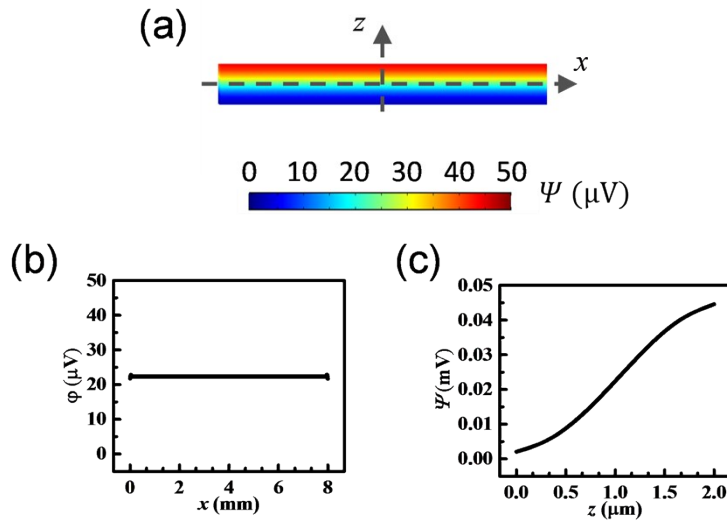


Fig. S9 (a) Electric potential distribution for membrane with $L=8$ mm, $h=2$ μm , $H=2$ μm . The thickness and length are not to scale. (b) Electric potential along the dashed line x in panel (a). (c) Electric potential along the dashed line z in panel (a).

Table S1. Summarized asymmetry ratio (H/h) and Photocurrent density of a series of geometry-asymmetric GOMs. The light intensity is kept at 100 mW cm⁻² under full-area irradiation with illumination duration time of 30 s in 10 μM KCl.

Asymmetry ratio (H/h)	1.01	1.14	1.76	1.97	2.35	2.57	2.84	3.16	3.34	3.63
Photocurrent density (μA cm ⁻²)	8.40	9.33	25.87	29.28	30.75	38.62	48.91	55.43	60.11	69.22

Table S2. Parameters used in the calculation

parameter	value	unit	meaning
ϵ	10	1	relative dielectric constant
μ_e	3.67×10^{-8}	$\text{m}^2/(\text{V} \cdot \text{s})$	electron mobility
μ_h	0	$\text{m}^2/(\text{V} \cdot \text{s})$	hole mobility
T	300	K	temperature
c_0	1.00×10^{-8}	mol/m^3	initial concentration
Z_h	1	e	hole charge
Z_e	-1	e	electron charge
h_0	5.2×10^{13}	$\text{m}^3/(\text{mol} \cdot \text{s})$	recombinant coefficient
g	1.67×10^{-8}	$\text{mol}/(\text{mW} \cdot \text{s} \cdot \text{m})$	generation coefficient
L_0	2.74	μm	light decay length

References

1. W. S. Hummers and R. E. Offeman, *J. Am. Chem. Soc.*, 1958, **80**, 1339-1339.
2. D. Li, M. B. Müller, S. Gilje, R. B. Kaner and G. G. Wallace, *Nat. Nanotechnol.*, 2008, **3**, 101.
3. D. R. Dreyer, S. Park, C. W. Bielawski and R. S. Ruoff, *Chem. Soc. Rev.*, 2010, **39**, 228-240.
4. J. Ji, Q. Kang, Y. Zhou, Y. Feng, X. Chen, J. Yuan, W. Guo, Y. Wei and L. Jiang, *Adv. Funct. Mater.*, 2017, **27**, 1603623.
5. J. Gao, W. Guo, D. Feng, H. Wang, D. Zhao and L. Jiang, *J. Am. Chem. Soc.*, 2014, **136**, 12265-12272.
6. B. Chitara, L. S. Panchakarla, S. B. Krupanidhi and C. N. Rao, *Adv. Mater.*, 2011, **23**, 5419-5424.
7. G. Venugopal, K. Krishnamoorthy and S.-J. Kim, *Appl. Surf. Sci.*, 2013, **280**, 903-908.
8. C. Y. Su, Y. Xu, W. Zhang, J. Zhao, A. Liu, X. Tang, C. H. Tsai, Y. Huang and L. J. Li, *Acs Nano*, 2010, **4**, 5285-5292.
9. C. Gomez-Navarro, R. T. Weitz, A. M. Bittner, M. Scolari, A. Mews, M. Burghard and K. Kern, *Nano Lett.*, 2007, **7**, 3499-3503.
10. R. S. Kajen, N. Chandrasekhar, K. L. Pey, C. Vijila, M. Jaiswal, S. Saravanan, A. M. H. Ng, C. P. Wong and K. P. Loh, *J. Appl. Phys.*, 2013, **113**, 063710.
11. G. A. Wetzelaer, L. J. Koster and P. W. Blom, *Phys. Rev. Lett.*, 2011, **107**, 066605.
12. A. K. Tripathi, D. C. Tripathi and Y. N. Mohapatra, *Phys. Rev. B*, 2011, **84**, 041201.
13. B. A. Ruzicka, S. Wang, L. K. Werake, B. Weintrub, K. P. Loh and H. Zhao, *Phys. Rev. B*, 2010, **82**, 195414.
14. C. Gómez-Navarro, R. T. Weitz, A. M. Bittner, M. Scolari, A. Mews, M. Burghard and K. Kern, *Nano Lett.*, 2007, **7**, 3499-3503.
15. A. B. Kaiser, C. Gómez-Navarro, R. S. Sundaram, M. Burghard and K. Kern, *Nano Lett.*, 2009, **9**, 1787-1792.
16. D. Joung and S. I. Khondaker, *Phys. Rev. B*, 2012, **86**, 235423.